Development of a Polar-Direct-Drive Design for Large Diameter Beryllium and Plastic Targets on the National Ignition Facility

Tyler Petrillo

Webster Schroeder High School

Advisor: Dr. R. S. Craxton

Laboratory for Laser Energetics

University of Rochester

Rochester, New York

June 2022

1. Abstract

A laser pointing design was developed for future experiments on the National Ignition Facility (NIF). Since the NIF is configured for indirect drive experiments, a method known as polar direct drive repoints the beams away from the center of the target to make direct drive experiments possible. The design was tailored for a beryllium target with a diameter of 4.5 mm, which is slightly larger than the diameter of typical targets imploded on the NIF. The 2D hydrodynamics simulation code SAGE was used to optimize the NIF beam parameters in order to maximize the uniformity of the target's implosion. The pointing design was also found to be optimal for plastic targets of an identical diameter. Additional simulations were carried out for a recent NIF shot in which the plastic target had substantial thickness variations. These simulations indicated that such thickness variations can significantly increase the implosion nonuniformity.

2. Introduction

Nuclear fusion combines two or more atomic nuclei to form a heavier nucleus, releasing a large amount of energy in the process. One method to achieve this reaction uses laser beams to irradiate a small fuel target comprising a shell that is typically filled with deuterium and tritium, two isotopes of hydrogen. The laser beams cause the outside of the shell to ablate outwards and the inside of the shell to compress inwards, bringing the deuterium and tritium to extremely high temperature and pressure. These conditions overcome the Coulomb repulsion forces between the positively charged nuclei, briefly allowing fusion reactions to occur. With ideal conditions, the newly formed helium nucleus would redeposit its energy into the fuel and create a chain of fusion reactions known as ignition. Ignition must occur in order to achieve breakeven, when the energy released by the fusion reactions exceeds the energy input by the laser beams. In order for laser fusion to be considered a viable energy source, however, the energy output must be approximately one hundred times greater than the energy input.

Currently, there are two different approaches to laser fusion: direct drive[1] and indirect drive.[2] In direct drive, as illustrated by Figure 1(a), laser beams are directly aimed at the target and the target is irradiated at normal incidence at all angles. The OMEGA laser system at the University of Rochester's Laboratory for Laser Energetics is configured for direct drive. This approach typically results in less uniform irradiation of the target than indirect drive. In indirect drive, as illustrated by Figure 1(b), the target is placed inside a cylindrical hohlraum, usually made of a metal with a high atomic number, such as gold. The beams enter through openings in the top and bottom of the hohlraum and hit the inner walls, which emit x rays that spread over a large part of the target's surface, uniformly irradiating the target. Despite the better uniformity of implosion offered by indirect drive, the target only absorbs about 20% of the laser energy.

Roughly 80% of the laser's energy is absorbed by the walls of the hohlraum or lost through the openings in the hohlraum. However, the increased uniformity of implosion and the large energy available at the National Ignition Facility (NIF) have enabled indirect drive to outperform direct drive to date. The NIF is currently configured for indirect drive.

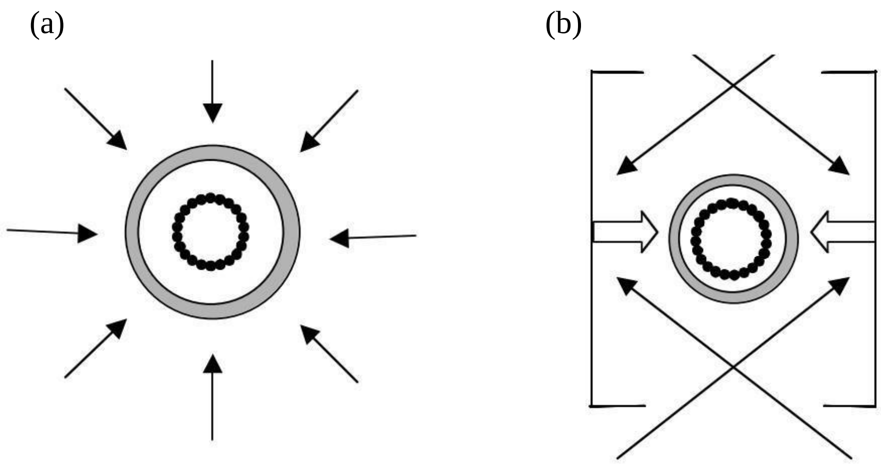

Figure 1. The two main approaches to inertial confinement fusion. (a) In direct drive, the laser beams directly hit the target and irradiate it. (b) In indirect drive, the beams enter a hohlraum, which emits x rays (represented by the clear arrows) that irradiate the target. [From Ref. 3]

The NIF's current configuration is not ideal for direct drive experiments. The NIF consists of 192 beams, divided amongst 48 quads of 4 beams each, located in 4 rings in each hemisphere at angles of 23.5°, 30.0°, 44.5°, and 50.0° from the vertical. If the NIF's beams were aimed at the center of the target, the energy deposited would not be evenly distributed over the target's surface. As shown in Figure 2(a), the poles compress much more than the equator. Therefore, in order to achieve a more uniform implosion, the drive on the equator must be increased to match the poles. A method called polar direct drive repoints the beams toward the equator, resulting in an increase in uniformity [Figure 2(b)].

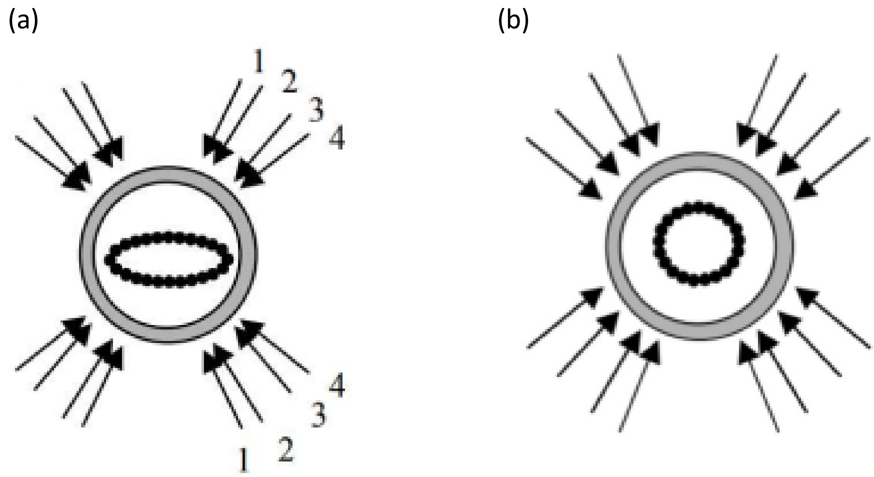

Figure 2. Two ways in which the NIF can be used to carry out direct drive experiments. (a) If the beams are fired towards the center of the target, the target's equator is undercompressed relative to its poles. Rings 1-4 are indicated. (b) Using polar direct drive, the target implodes much more uniformly. [From Ref. 3]

Depending on the size of the target being imploded, the NIF's beam parameters need to be adjusted in order to optimize the uniformity of the target's implosion. For a proposed beryllium target, which is 4.5 mm in diameter, using the optimized pointings designed for a smaller target would result in undercompression at the equator, leading to less overall uniformity. Developing a pointing design specific to this size target is essential for maximizing its uniformity as it implodes. This work assumes the use of the NIF's current set of phase plates, optics which spread the energy of the laser beam to produce a more uniform beam after focusing, and optimizes other key NIF beam parameters. One of such parameters is the defocus on each ring of beams. By moving the focus lens toward the target (defocusing the beam), the size of the beam spot created on the target increases while the intensity of the spot decreases. Each ring of beams can also be shifted away from the center of the target in both the θ and ϕ directions. The polar angle, θ, increases from 0° at the chamber top to 180° at its bottom. The azimuthal angle, ϕ, ranges from 0 to 360° anticlockwise, when viewed from the chamber top. Each beam can be shifted to a specific angle in the θ direction, while each of the beams in a ring can be spread out horizontally in the ϕ direction.

The primary goal of this work was to create a set of pointings which maximized the implosion uniformity of the proposed 4.5 mm beryllium target (Section 3). This design was also found to be suitable for plastic targets of similar size (Section 4). The report also explores how thickness variations in a target's surface, modeled by Legendre polynomials, can significantly impact uniformity as the target implodes (Section 5).

3. Optimized Design

The optimized design was intended to maximize the uniformity of the target's implosion right before fusion reactions occur. The target is a shell of 15 μm of beryllium (Be) with a diameter of 4.46 mm. The laser pulse used on this target is shown in Figure 3. The laser pulse delivers 1.6 MJ with a linear rise to 427 TW at 1.7 ns and a linear fall from 4.5 ns to 4.7 ns. The optimized design was largely based on a previous design (Orange[4]) that was optimized for targets of 4 mm in diameter.

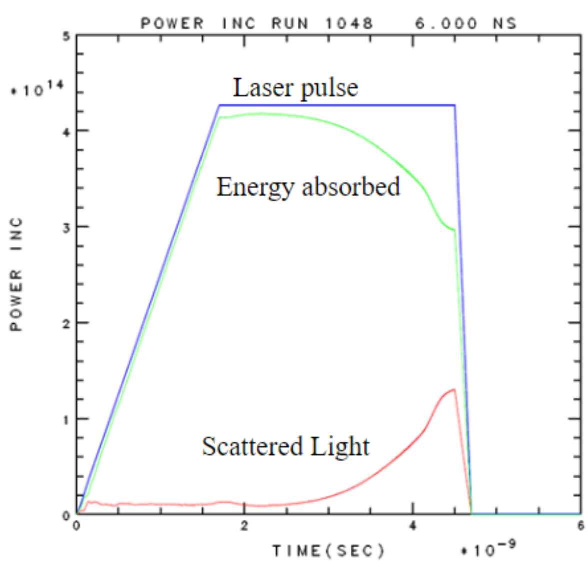

Figure 3. Power vs. time graph of the optimized design showing the incident laser pulse, energy absorbed, and transmitted power in W.

The implosion of the shell and the incoming rays from a Ring 4 beam are shown in Figure 4. The figure shows a raytrace plot of the optimized design at 3 ns. The heavy outer semicircle at a radius of 2.23 mm represents the target's initial position before it was hit by the laser pulse, while the inner heavy semicircle illustrates how far the shell has moved through 3 ns. The rays near normal incidence have had their energy almost completely absorbed by the target.

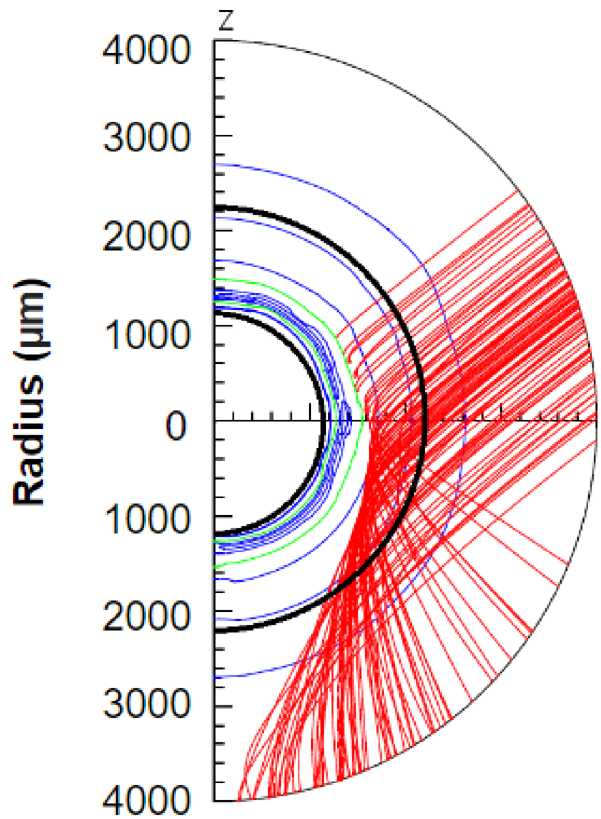

Figure 4. Raytrace of the bottom-right beam of Ring 4 at 3 ns of the optimized design. Electron density contours are shown by the blue circular lines, which show increasing density as the blue semicircles decrease in radius. The green lines represent the critical density, the density beyond which laser light cannot propagate. The vertical axis measures distances in µm. [Run 1048]

The imploding shell in Figure 4 appears very uniform. To examine this more closely, the center of mass radius of the imploding shell is plotted as a function of angle θ from the z axis in Figure 5. The figure shows the optimized design and the Orange target design on the 4.46 mm Be target at 3 ns. Like Figure 4, the figure comes from a 2D calculation and therefore represents averages over the azimuthal angle ϕ. At 3 ns, the target is around 1450 µm away from its center. The overall velocity nonuniformity of the optimized design in the θ direction improved over the Orange design by nearly two fold (see Sec. 3.2).

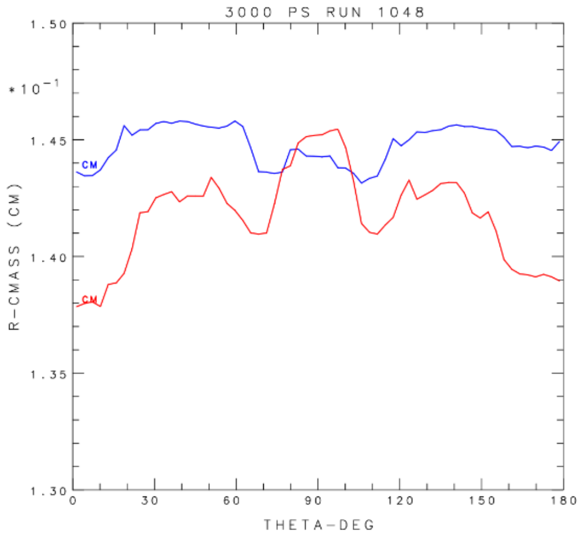

Figure 5. Center-of-mass radius (cm) vs. θ (degrees) at 3.0 ns of the optimized design (in blue) and the Orange target design (in red) for a 4.5 mm diameter target. [Runs 1002, 1048]

Figure 6 shows the 3D center-of-mass contour plot at 3 ns using the optimized design. It comes from taking the azimuthal average from Figure 5, and adding the azimuthal variations using the 3D deposition pattern of laser energy [following Ref. 4]. The overall velocity nonuniformity (see Sec 3.2) is just 1.65%.

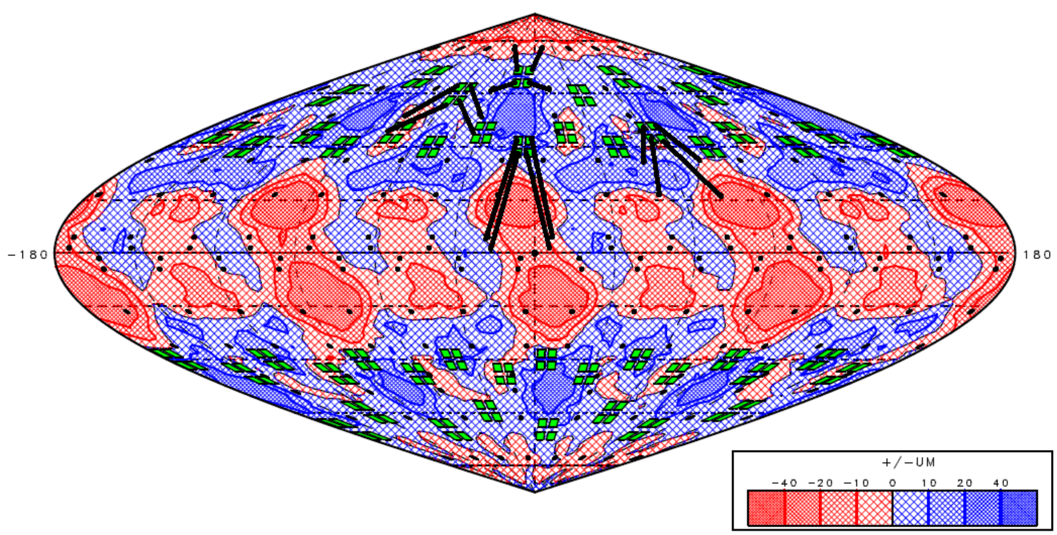

Figure 6. The 3D center-of-mass plot of the optimized design at 3 ns with contours indicating deviations from the average radius of the beryllium shell in μm. Red regions represent overcompression and blue regions indicate undercompression. The green squares represent the four beams in each quad and the black dots represent where each beam has been repointed to. The black lines show how the laser beams in four representative quads are repointed to maximize uniformity. [Run 1048]

3.1 Pointings and Defocusing

The pointings in the θ and ϕ directions and defocus distances for the previous (Orange) and optimized designs are shown in Table 1. The optimized pointings in both the θ direction and the ϕ direction have been adjusted in order to maximize uniformity. The left beams of each quad are moved Δϕ to the left and the right beams are moved Δϕ to the right relative to the center of each quad. There are no pointings in any of the 4 rings on the NIF that were shifted more than 5° compared to the previous design.

	Orange Design θ	Orange Design Δϕ	Orange Defocus (cm)	Optimized Design θ	Optimized Design Δϕ	Optimized Defocus (cm)
Ring 1 top beams	13°	22.5	2.5	13°	22.5	3.25
Ring 1 bottom beams	24°	22.5	2.5	28°	22.5	3.25
Ring 2 top beams	38°	22.5	2.0	38°	22.5	3.00
Ring 2 bottom beams	46°	22.5	2.0	44°	22.5	3.00
Ring 3 top beams	53°	11.25	2.0	55°	12.5	3.00
Ring 3 bottom beams	71°	11.25	2.0	68°	12.5	3.00
Ring 4 top beams	79°	11.25	2.0	84°	12.0	3.00
Ring 4 bottom beams	88°	15.0	2.0	88°	11.0	3.00

Table 1: Beam parameter specifications for all 4 Rings of the Orange and optimized designs. All the optimized pointings changed very little from the previous design. The most significant changes were shifting the Ring 4 top beams in order to increase drive on the equator and increasing the defocus to reduce azimuthal nonuniformity for the larger target.

The Orange design resulted in undercompression at the equator on the larger 4.46 mm Be target (see Fig. 5). To increase the drive on the equator, the ring 4 top beams were shifted from 79˚ to 84˚. Consequently, the drive away from the equator ($\theta \approx 60^\circ$) was reduced. To compensate for this change, the ring 3 bottom beams were shifted from 71˚ to 68˚. The changes made to the other beams in the θ direction slightly improved azimuthal uniformity. Changes made in the ϕ direction were less significant than in the θ direction. Only the pointings of Rings 3 and 4 were shifted to increase uniformity. The Orange design set ring 3 and the top of ring 4 beams to 11.25˚ in order to maintain uniformly distributed energy in the ϕ direction. However, the optimized design set ring 3 beams to 12.5˚ and the top of ring 4 beams to 12˚, which resulted in a slightly higher uniformity in the ϕ direction. Overall, any changes made in the ϕ direction had a minimal impact on the overall uniformity of the target's implosion. The optimized design also set the $\Delta\phi$ of the ring 4 bottom beams to 11˚.

Defocusing is used to change the size of each beam spot of the laser. This is done by moving the focus lens toward the target. Since the proposed 4.46 mm Be target is slightly larger than the 4 mm targets that the Orange pointings were tailored for, the defocus of each beam had to be increased in order to reduce nonuniformity in the azimuthal direction. The defocus for rings 2, 3, and 4 was set to 3 cm, while the defocus for ring 1 beams was set to 3.25 cm. This is a significant increase over the Orange design, which had a maximum defocus of 2.5 cm for any given ring. The maximum allowed defocus using the NIF's current phase plates is roughly 3.5 cm, which makes it difficult to optimize larger targets than 4.5 mm in diameter.

3.2 Improved Uniformity

The optimized design maintained a high absorption of beam energy across the target's surface. Although a large portion of the rays are deflected in Figure 4, they still deposit a large amount of their energy into the target. Averaged over the entire laser pulse, the target has an overall energy absorption of 91.3%, which is slightly less than the 94.1% energy absorption when using the Orange target design.

The optimized design, as shown in Figures 4 and 5, produced a high degree of uniformity in the θ direction, allowing the equator to compress uniformly at the same rate as the poles. The optimized design produced a root-mean-square (rms) variation in center of mass radius, relative to the average radius, of 0.58% through 3 ns. Another useful quantity for evaluating the uniformity of a target's implosion is the rms nonuniformity of the average velocity (Δv-rms), which is calculated by dividing the rms of deviations in the center of mass radius by the distance that the target has traveled. At 3 ns, the target has moved an average of 776 μm and the rms deviation in the distance moved is just 8.4 μm, leading to a Δv-rms of 1.08% (Figure 5) in the θ direction. The optimized design has shown substantial improvement over the Orange target design (Δv-rms = 2.06%) by reducing overall nonuniformity on the proposed target by nearly a factor of two. The changes made to the pointing and defocusing (Section 3.1) significantly strengthened the equator, as evident by the red regions between θ=70˚ and θ=110˚ in Figure 6. Additionally, there are no places on the target that deviate from the average radius of the beryllium shell by more than ±40 μm.

The relationship between the components of velocity nonuniformity in the θ and ϕ directions is given by the equation

$$(\Delta v - rms)^2 = \left(\Delta v - rms(\theta)\right)^2 + \left(\Delta v - rms(\phi)\right)^2 \tag{1}$$

where Δv-rms is the total nonuniformity, Δv-rms(θ) is the nonuniformity in the θ direction, and Δv-rms(ϕ) is the nonuniformity in the ϕ direction. The optimized design has an overall Δv-rms of 1.65% at 3 ns. Knowing the Δv-rms(θ), Equation 1 can be used to calculate the Δv-rms(ϕ). The optimized design has a Δv-rms(ϕ) of 1.25%, which is slightly higher than the 1.08% Δv-rms(θ) nonuniformity. The overall Δv-rms is nearly a two-fold improvement over the Orange target design for which the Δv-rms is 3.06%.

3.3 Ideal Laser Pulse and Thickness

The optimized design was intended for a laser pulse that delivered 1.6 MJ of energy. The proposed Be target was observed to have imploded before the end of the laser pulse, wasting energy in the process. The duration of the laser pulse can be shortened in order to save energy. Alternatively, the extra energy can be used to implode a slightly thicker target, which would also increase the total amount of energy absorbed by the target.

Figure 7 illustrates the implementation of a shorter laser pulse on the proposed target. The laser pulse depicted in Figure 7 is identical to the original 1.6 MJ laser pulse (Figure 3), except that the laser experiences an earlier linear fall from 4.0 to 4.2 ns. Using the shortened laser pulse in Figure 7, the target now has a higher energy absorption of 94.9%. Since the bang time, the time at which fusion reactions occur, is estimated to occur at roughly 4.0 ns, this change in the duration of the laser pulse is unlikely to have any effect on the neutron (energy) yield.

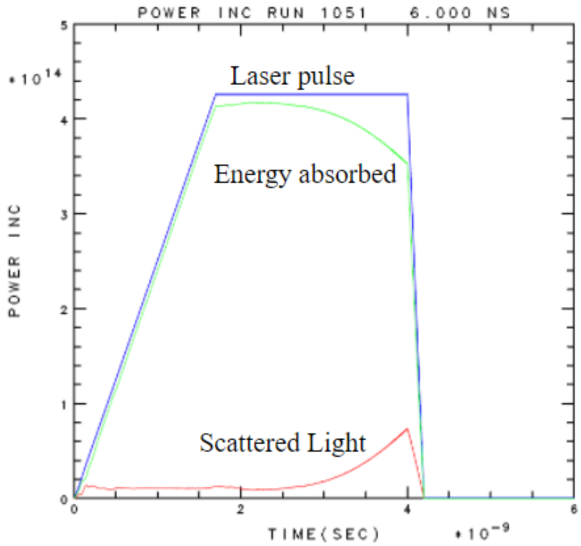

Figure 7. Power vs. time graph for the optimized design using the modified 1.3 MJ laser pulse, which experiences an earlier linear fall from 4.0 to 4.2 ns. The shorter laser pulse increased the percentage of energy absorbed by the target from 91.3% (Figure 3) to 94.9%.

A target with a thicker shell can be used to slow the rate at which the target implodes. Figure 8 depicts the power vs. time graph of a 20 µm beryllium target, which is 5 µm thicker than the proposed beryllium target used in Figure 3. The additional beryllium causes the target to implode slower than the proposed target. The bang time can be approximated to between 4.5 and 5 ns, which is at roughly the same time that the laser powers off. The overall energy absorption is 95.8%. Increasing the thickness of the shell enables higher energy absorption without the need to reduce the duration of the laser pulse. Although this simulation used the Orange design, the same result would be expected for the optimized design.

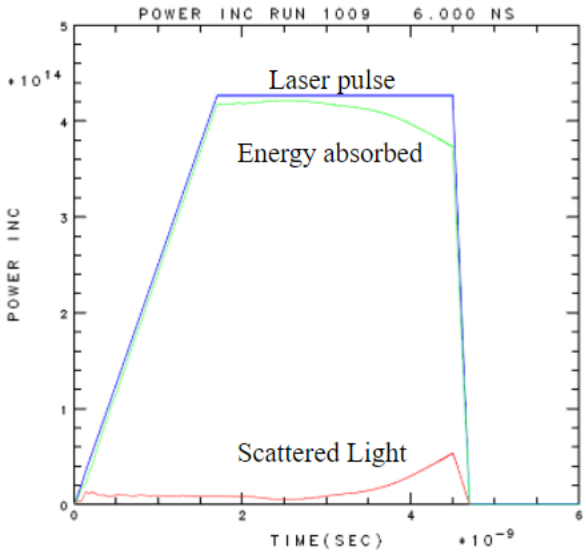

Figure 8. Power vs. time graph for a 20 μm Be target using the Orange design and a 1.6 MJ laser pulse. The overall energy absorption is 95.8%.

4. Optimized Design for Plastic Targets

Targets designed for inertial confinement fusion are made out of a variety of materials. A common material for these targets is plastic (CH), which has a density of 1.044 g/cm^3. CH has a noticeably lower density than beryllium (Be), which has a density of 1.85 g/cm^3 and is also the material that the optimized design was created for. A plastic target will compress faster than a beryllium target of the same thickness.

Figure 9 compares the uniformity of the proposed Be target (15 μm in thickness) to two CH targets of differing thicknesses. Through 3.0 ns, the 21 μm CH target (blue line) has a Δv-rms of 1.08% in the θ direction, which is identical to that of the 15 μm Be target that the pointings were optimized for. Similarly, the 27 μm CH target, which has not moved as far as the other 2 targets through 3.0 ns, produced a Δv-rms of 1.51% in the θ direction. The similar uniformity performance for both CH thicknesses suggests that the optimized design suits CH as well as Be.

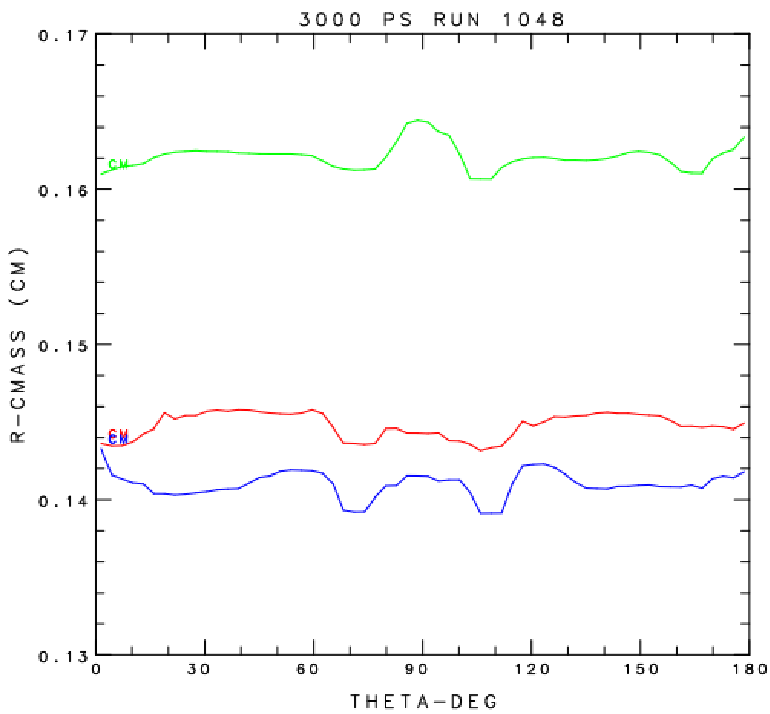

Figure 9. Center-of-mass radius (cm) vs. θ (degrees) at 3.0 ns for three targets of diameter 4.5 mm using the optimized pointing design. The red line is identical to the blue line from Figure 5, allowing for the different scale on the y-axis. The green and blue lines represent CH targets with thicknesses of 27 µm and 21 µm, respectively [Runs 1048, 1055, 1061]

The equivalent mass for 15 µm of Be is 23.7 µm of CH. However, the 15 µm Be target and 21 µm CH target have moved approximately the same distance through 3.0 ns, and are currently both 0.14 cm from their centers. This would suggest that a mass equivalent CH target (23.7 µm) would move slower than the Be target, and that CH compresses slower than Be.

For a plastic target to make use of the entire 1.6 MJ laser pulse, an ideal thickness must be found. The power vs. time graph in Figure 10 illustrates the 1.6 MJ laser pulse on a CH target that is 30 µm thick. The target absorbed 94.8% of the total laser energy and had an estimated bang time between 4.5 ns and 5.0 ns. Laser energy that is used after fusion reactions occur does not contribute to the energy (neutron) yield, and also has the potential to damage laser optics. By selecting a CH thickness of 30 µm, the laser will turn off roughly at the time of the bang, thus minimizing energy loss.

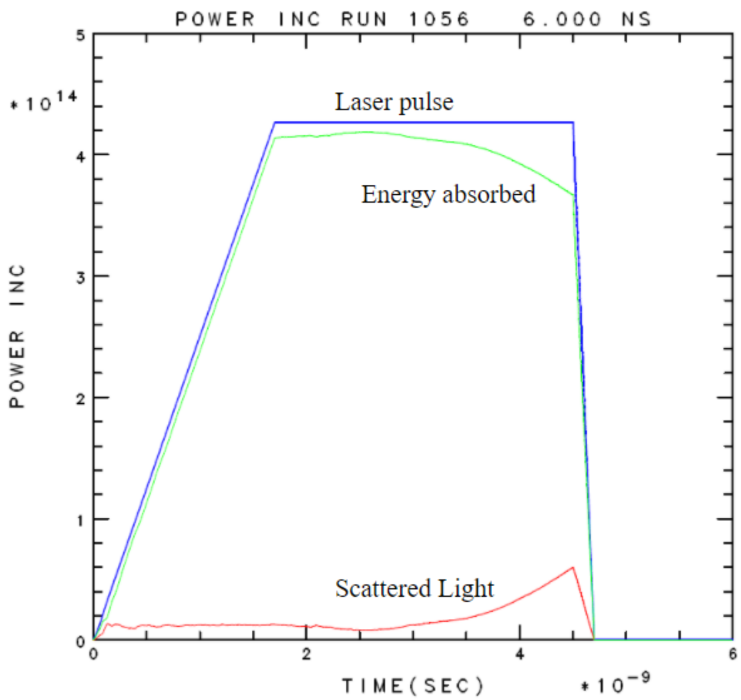

Figure 10. Power vs. time graph for a 30 µm thick CH target using the optimized pointing design. The laser pulse contains a total of 1.6 MJ of energy and has a duration of 4.7 ns. The laser pulse peaks at roughly 430 TW of power. [Run 1056]

5. Thickness Variations

In a recent polar direct drive experiment on the NIF (N210627-001), a plastic (CH) target with a radius of 4.3 mm was observed to have a thickness that varied between 19.8 µm and 28.1 µm, which amounts to an 8.3 µm difference in thickness. Errors in target thickness are certainly decreasing the target's uniformity as it implodes, but the degree to which this particular target's uniformity was affected remains unknown.

5.1 Modeling Thickness Errors

One way that thickness variations can be modeled is through the use of Legendre polynomials, which are a system of complete and orthogonal polynomials. The first five Legendre polynomials, which have been reparametrized in terms of angles, are shown in Figure 11. Each polynomial is graphed from 0 to 180˚ to represent the θ direction across a target's surface.

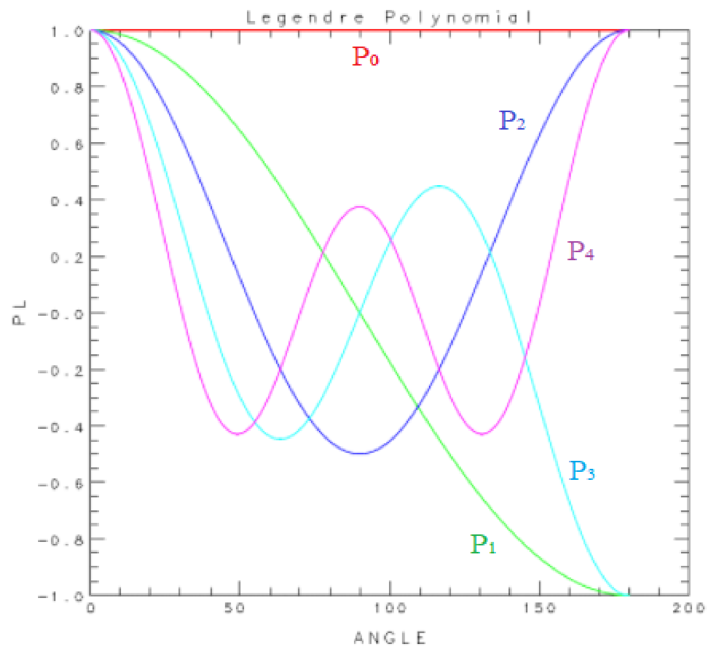

Figure 11. The first five Legendre polynomials P_n (up to n = 4) from 0 to 180 degrees are labeled on the left. Each polynomial ranges from -1 to 1 along the vertical axis, which has dimensionless units. Each graph illustrates how a thickness variation can be distributed across a target's surface.

5.2 Analyzing Thickness Variations

Several 2-D hydrodynamic simulations were run using the code SAGE that applied Legendre polynomial variations to a plastic target. Each simulation used a target with a diameter of 4.3 mm (the same as shot N210627-001) and an average thickness of 25 µm, creating plots with 2 µm (25 ± 1 µm) and 8 µm (25 ± 4 µm) thickness differences.

In the simulations of the 4.3 mm plastic target that contained Legendre polynomial variations, an increase in nonuniformity was evident. After applying P_3 Legendre polynomial variations to the plastic target, Figure 12 (a) indicates that a 2 µm difference produces noticeable nonuniformities. At 0˚ in the θ direction, the innermost density contour is roughly 800 µm away from the target center. At the opposite pole (θ = 180˚), the contour is only 600 µm away from the center.

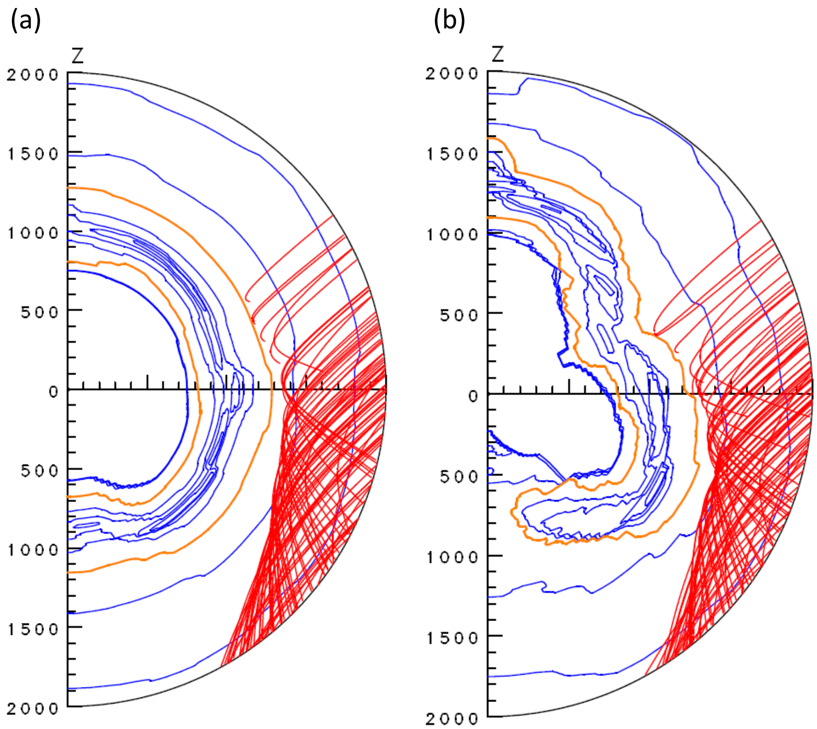

Figure 12. Raytrace plots of P_3 Legendre polynomial variations applied to a 2 μm difference (a) and an 8 μm difference (b) at 3.5 ns. The density contours in (a) reveal some nonuniformity, while the nonuniformities in (b) are more pronounced. [Runs 1043, 1037]

As expected, the target with an 8 μm variation in its thickness was significantly less uniform than its 2 μm variation counterpart. In Figure 12 (b), the target has compressed more unevenly, as evident by its behavior at the poles. At 0˚, the innermost contour is 1000 μm away from the center. Conversely, the opposite pole is close to 200 μm away from the center. Other regions of the target are also significantly nonuniform. The target is significantly overcompressed around 60˚ from the vertical, but undercompressed at roughly 120˚ from the vertical. Such distortion can be expected to significantly lower the neutron yield.

Simulations that applied other Legendre polynomial modes yielded similar results. After applying P_2 Legendre polynomial variations to the plastic target, Figure 13 shows a plot of the center-of-mass radius vs. θ that compares a target with no thickness variations to two targets that contained 2 μm and 8 μm thickness variations. Through 3.0 ns, the plastic target with no thickness variations has a Δv-rms of 1.59% in the θ direction, while the 2 μm target has a Δv-rms of 2.37%. The 8 µm difference target has an exceptionally high Δv-rms of 11.11% in the θ direction.

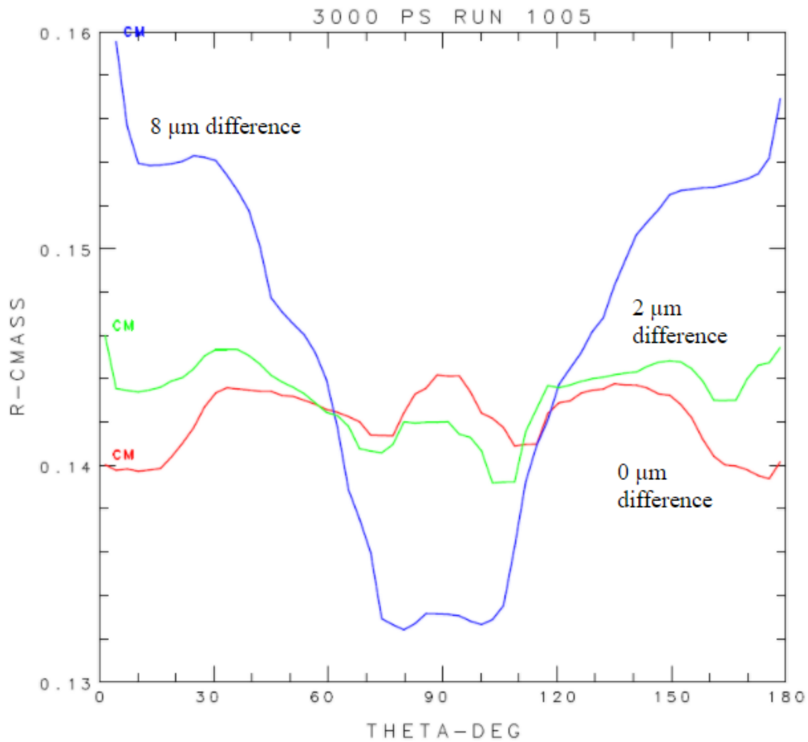

Figure 13. Center-of-mass radius (cm) vs. θ (degrees) at 3.0 ns for three different thickness variations with applied P_2 Legendre polynomials. The 0 µm, 2 µm, and 8 µm differences are represented by the red, green, and blue lines, respectively. [Runs 1005, 1023, 1042]

The target with a 2 µm difference saw less than a 1% increase in its Δv-rms nonuniformity compared with the target with no thickness variations, suggesting that small variations in thickness do not have a significant impact on the overall uniformity. However, the target with an 8 µm difference experienced a 9.52% increase in its nonuniformity, which resulted in significant distortion of the target's surface. Due to the nature of the Legendre polynomial used, the target's surface resembles a parabola, as shown by the blue line in Figure 13. The behavior of the 8 µm difference target shows how easily thickness variations can be amplified as the target implodes. Therefore, in order to maintain a high level of uniformity, a target's variations in thickness need to be as minimal as possible.

6. Conclusion

An optimized design was developed to maximize uniformity for a Be target that is 4.5 mm in diameter. By increasing the defocus of each beam and making slight changes to the pointings in both the θ and ϕ directions, the overall uniformity improved by nearly two-fold over a previous design. The optimized design produced similar improvements on CH targets, making the design suitable for targets of both materials. An ideal shell thickness and laser pulse duration were found to maintain low nonuniformity and improve energy absorption. Variations greater than 2 μm in a target shell's thickness had a significant impact on uniformity, posing a need to limit these variations.

7. Acknowledgements

I would like to thank my family for their unwavering support throughout the program. I'd also like to thank my high school math and science teachers for encouraging me to continue my pursuit of knowledge. Lastly, I'd like to thank my advisor Dr. R.S. Craxton for his help and flexibility, and for providing me this amazing opportunity.

8. References

1. J. Nuckolls, et al., "Laser Compression of Matter to Super-High Densities: Thermonuclear (CTR) Applications," Nature **239**, 139 (1972).

2. J.D. Lindl, "Development of the Indirect-Drive Approach to Inertial Confinement Fusion and the Target Physics Basis for Ignition and Gain," Phys. Plasmas **2**, 3933 (1995).

3. A. M. Cok, "Development of Polar Direct Drive Designs for Initial NIF Targets," Laboratory for Laser Energetics High School Research Program (2006).

4. C.B. Yeamans, et al., "High yield polar direct drive fusion neutron sources at the National Ignition Facility," Nucl. Fusion **61** 046031 (2021).